ARTICLE

Novel Evolution Process of Zn-Induced Nanoclusters on Si(111)-(7×7) Surface

Changjie Zhou · Yaping Wu · Xiaohang Chen · Wei Lin · Yinhui Zhou · Junyong Kang · Huili Zhu

Abstract A tiny number of Zn atoms were deposited on Si(111)-(7×7) surface to study the evolution process of Zn-induced nanoclusters. After the deposition, three types (type I, II, and III) of Zn-induced nanoclusters were observed to occupy preferably in the faulted half-unit cells. These Zn-induced nanoclusters are found to be related to one, two, and three displaced Si edge adatoms, and simultaneously cause the depression of one, two, and three closest Si edge adatoms in the neighboring unfaulted half-unit cells at negative voltages, respectively. First-principles adsorption energy calculations show that the observed type I, II, and III nanoclusters can reasonably be assigned as the Zn_3Si_1, Zn_5Si_2, and Zn_7Si_3 clusters, respectively. And Zn_3Si_1, Zn_5Si_2, and Zn_7Si_3 clusters are, respectively, the most stable structures in cases of one, two, and three displaced Si edge adatoms. Based on the above energy-preferred models, the simulated bias-dependent STM images are all well consistent with the experimental observations. Therefore, the most stable Zn_7Si_3 nanoclusters adsorbed on the Si(111)-(7×7) surface should grow up on the base of Zn_3Si_1 and Zn_5Si_2 clusters. A novel evolution process from Zn_3Si_1 to Zn_5Si_2, and finally to Zn_7Si_3 nanocluster is unveiled.

Keywords Nanoclusters · Silicon · Scanning tunneling microscopy · First-principles calculations

1 Introduction

Design and fabrication of nanoclusters is a new inspiring field because of their amazing features that are remarkably different from classical materials [1–4]. The beneficial electronic, optical, magnetic, and chemical properties of nanoclusters can be employed in many fields, such as optoelectronic devices [5, 6], single-electronic devices [7], ultrahigh-density magnetic recording [8–10], and quantum computing. From the viewpoint of practical applications, it is necessary to fabricate stable, ordered, and identical-sized nanoclusters. In the past decade, utilizing the natural template of Si(111)-(7×7) surface, a number of metal nanoclusters with identical sizes and shapes have been successfully fabricated, such as group IA metals (Na) [11, 12], group IB metals (Au) [13], group IIB metals (Zn) [14], group IIIA metals (Al, Ga, Tl, and In) [15–20], group IV metals (Pb) [21], and even some 3d ferromagnetic metals (Fe, Co, and Ni) [22–24]. By using the ultrahigh-vacuum (UHV) scanning tunneling microscopy (STM) technology combined with the first-principle theoretical simulations, the stable structural configurations of the identical-sized nanoclusters on Si(111)-(7×7) surface have been clearly illustrated. It was found that the atomic structures of these identical-sized nanoclusters had a characteristic of the varying valence. For instance, group IIIA metals (Al, Ga, and In) tend to form the stable Al_6Si_3, Ga_6Si_3, and In_6Si_3 nanoclusters with six metal atoms and three displaced Si

C. Zhou · Y. Wu (✉) · X. Chen · W. Lin · Y. Zhou · J. Kang (✉)
Fujian Key Laboratory of Semiconductor Materials and Applications, Department of Physics, Xiamen University, Xiamen 361005, People's Republic of China
e-mail: ypwu@xmu.edu.cn

J. Kang
e-mail: jykang@xmu.edu.cn

C. Zhou · H. Zhu
Department of Physics, School of Science, Jimei University, Xiamen 361021, People's Republic of China

edge adatoms connecting as a hollow triangle [15–20]. However, group IIB metal, Zn, tends to form the stable Zn_7Si_3 nanoclusters with an excess Zn atom characteristically occupying the center of the hollow triangle [14]. Although the structural configurations have been clearly clarified, the evolution process of these metal nanoclusters was rarely addressed. That is, how these nanoclusters gradually evolve and finally grow up to the intact Ga_6Si_3 or Zn_7Si_3 nanoclusters? For the controlled synthesis and device design, it is desirable to carefully investigate the evolution process of metal nanoclusters on Si(111)-(7×7) surface.

In this paper, three types of Zn-induced nanoclusters were grown at room temperature on the clean Si(111)-(7×7) surface with a tiny number of Zn atoms. Using in situ STM technology for real-space imaging, these nanoclusters are systematically characterized at both the positive and negative bias voltages. Taking into account the adsorption energies of different structural models derived from the first-principles calculations, the experimental atomic configurations of these three types of nanoclusters are identified to be Zn_3Si_1, Zn_5Si_2, and Zn_7Si_3. Furthermore, these structures are further confirmed by theoretically simulated STM images. Accordingly, a novel evolution process from Zn_3Si_1 to Zn_5Si_2, and finally to Zn_7Si_3 nanocluster is unveiled.

2 Methods

The experiments were performed within an ultrahigh-vacuum system (OMICRON MBE-SPM system) which consists of a growth chamber and an analysis chamber with a base pressure of about 2.0×10^{-10} mbar. Atomically clean Si(111)-(7×7) surface was prepared by standard flashing to about 1200 °C while keeping the vacuum at a pressure better than 1×10^{-9} mbar [21]. High-purity Zn (99.9999 %) was evaporated from a boron nitride crucible onto the Si(111)-(7×7) surface. A tiny number of Zn atoms were deposited through the control of Zn source temperature and evaporation time. The sample was then transferred to the analysis chamber and imaged by an OMICRON STM using chemically etched tungsten tips [25, 26]. All STM images reported here were recorded under a constant tunneling current of 0.05 nA.

In order to identify the structural configurations of the observed nanoclusters, the adsorption energies and STM images were calculated by the first-principles simulations within the framework of the generalized gradient approximation [27, 28], using the plane-wave density functional theory Vienna Ab Initio Simulation Package [29–31]. The structural models were periodically repeated by an atomic slab consisting of 4 Si layers (200 Si atoms), with

n Zn atoms adsorbed on the top and 49 H atoms bonded at the bottom. A 12-Å-thick vacuum layer was applied for separating the slabs to form a surface. Ionic potentials were described by ultrasoft pseudopotentials, and the plane-wave cutoff energy was set at 330 eV. The surface Brillouin zone was sampled at the point only. The Zn-$3d4s$ and Si-$3s3p$ were employed as the valence electrons. Structural optimizations were carried out by relaxing all the atomic geometries using the conjugate gradient algorithm [32]. The forces on all the atoms were converged within 0.01 eV/Å.

3 Results and Discussion

For observing the evolution process of Zn-induced nanoclusters, a tiny number of Zn atoms were deposited on the clean Si(111)-(7×7) surface, as shown in Fig. 1a. The faulted (F) and unfaulted (U) triangular halves of 7×7 unit cell are denoted separately in the surface. Due to the different atomic structures in two triangular halves [33], Si adatoms in the faulted half-unit cells (FHUCs) show a little brighter than that in the unfaulted half-unit cells (UHUCs) at the negative bias voltages, as shown in Fig. 1. After Zn deposition, three types of Zn-induced nanocluster structures appear on the surface, as denoted, respectively, by the green (type I), pink (type II), and blue (type III) triangles in Fig. 1b and c. Most of the nanoclusters are observed to adsorb on the FHUCs of the Si(111)-(7×7) surface. This preference is attributed to the lower adsorption energy in the FHUC for the dimer-adatom-stacking (DAS) fault model of the Si(111)-(7×7) surface [33]. For the filled-state STM images of type I nanoclusters, as shown in Fig. 1b, it seems that one Si edge adatom is pushed toward the center of the FHUC. And one closet Si edge adatom in the neighboring UHUC becomes dark as denoted by a green dotted circle. For the filled-state STM images of type II nanocluster, as shown in Fig. 1c, it exhibits a triangular big bright dot in the center of the FHUC. Moreover, careful comparison shows that two closet Si edge adatoms in the neighboring UHUCs become dark, as denoted by the pink dotted circles. For type III nanocluster, as shown in Fig. 1b and c, it is also apt to occupy the center of FHUC with a bright triangular morphology in filled-state STM images. Simultaneously, the three closet Si edge adatoms in the neighboring uncovered UHUCs are almost darkened, as indicated by the blue dotted circles. It is thus clear that the formation of type I, II, and III nanoclusters causes, respectively, one, two, and three darkened closest Si edge adatoms in neighboring UHUCs in the filled-state STM images. Therefore, three types of Zn-induced nanoclusters should have the similar formation mechanism in the atomic configurations.

To better understand the gradual evolution process of Zn-induced nanoclusters, we systematically studied the

196

Nano-Micro Lett. (2015) 7(2):194–202
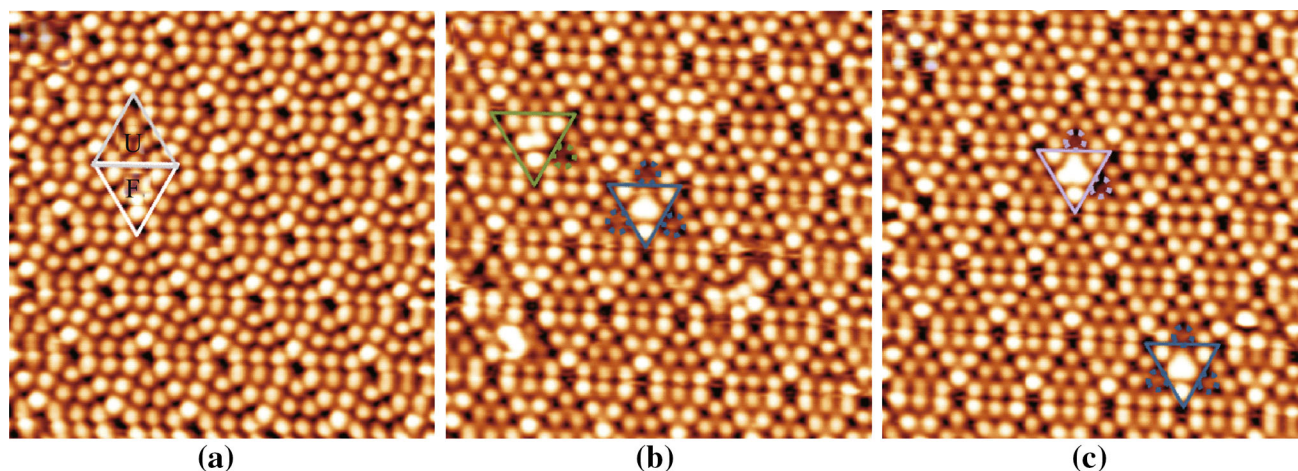
Fig. 1 The filled-state STM images of Si(111)-(7×7) surface **a** before the deposition of Zn atoms ($V_S = -0.5$ V, 15 nm × 15 nm) and **b, c** after a tiny number of Zn atoms were deposited ($V_S = -1.5$ V, 15 nm × 15 nm). The faulted (F) and unfaulted (U) triangular halves of 7×7 unit cell are denoted separately. Three types of Zn-induced nanoclusters observed in **b** and **c** are denoted, respectively, by the *green* (type I), *pink* (type II), and *blue* (type III) *triangles*. The *darkened closet* Si edge adatoms in neighboring UHUCs are denoted, respectively, by the *green*, *pink*, and *blue* *dotted circles*. (Color figure online)

geometric structures of three types of observed nanoclusters. A series of empty- and filled-state STM images were taken at different bias voltages of +1.5, +1.0, +0.5, −0.5, −1.0, and −1.5 V on the same surface area with one Zn-induced nanocluster in the FHUC, as shown in Fig. 2. For type III nanocluster, two groups of empty- and filled-state STM images shown in Fig. 2a–d exhibit almost the same topographic evolution as the previous research [14]. Combined with the results of the simulated STM images as shown in Fig. 5, we deduce that type III nanoclusters should be the Zn_7Si_3 nanoclusters. The structural configuration of Zn_7Si_3 nanocluster, as shown in Fig. 3d, exhibits that three adsorbed Zn atoms replace the three Si edge adatoms in the FHUC, meanwhile the replaced Si atoms and other three Zn atoms connect into a hexagon, with another characteristic Zn atom occupying the center. Considering the observed STM images and the structural configuration results, we deduce that the depression of the three closet Si edge adatoms in neighboring UHUCs, as shown in the filled-state STM images in Fig. 2b and d, is attributed to three displaced Si edge adatoms in the FHUC. That is, when one Si edge adatom in the FHUC is replaced by Zn atoms, the closet Si edge adatom in neighboring UHUC exhibits a darkened filled-state STM image.

For type I nanocluster, denoted by the green triangle, it exhibits a "U" shape pattern in the center of FHUC at the bias voltage of +1.5 V. Then the cluster changes to the pattern consisting of two bright and one dim dots at the bias voltage of +1.0 V. Different from the "U" shape pattern, the cluster exhibits a "V" shape pattern at the bias voltages of −1.5 and −1.0 V. As the voltage further reduces to ± 0.5 V, the cluster images transform to the pattern

with two bright dots and one vanished Si edge adatom. Careful observation shows that the two bright dots should come from the two unaltered Si edge adatoms. Therefore, the formation of type I nanocluster is relative to one Si edge adatom and none of the other two intact Si edge adatoms in the FHUC. In the empty-state STM images, three closet Si edge adatoms in the neighboring UHUCs are almost unaltered as compared with the clean Si(111)-(7×7) surface. As for the negative voltage of −0.5 V, one of the three closet Si edge adatoms exhibits a dark image, as marked by a green dotted circle in Fig. 2b, whose position is just opposite of the disappeared Si edge adatom in the FHUC. Since one displaced Si edge adatom in the FHUC would induce the depression of the closet Si edge adatom in neighboring UHUC in the filled-state STM image, the formation of type I nanocluster is obviously relative to one displaced Si edge adatom in the FHUC and the other two Si edge adatoms are almost kept unaltered. The observed dim dot at the bias voltage of +1.0 V, as shown in Fig. 2a, should be the displaced Si edge adatom. However, due to the uncertainty of the number and the position of adsorbed Zn atoms, the structural configuration of type I nanocluster is still not clear. Therefore, it is necessary to further employ the theoretical calculation and simulation, which would be discussed below.

Type II nanocluster, denoted by the pink triangle, shows a shape of isosceles triangle at the bias voltage of +1.5 V. As the voltage reduces from +1.5 to +0.5 V, the size and brightness of the base of isosceles triangle decrease gradually. And the cluster transforms to the pattern with one bright dot and two vanished Si edge adatoms. Careful observation shows that the bright dot should come from the
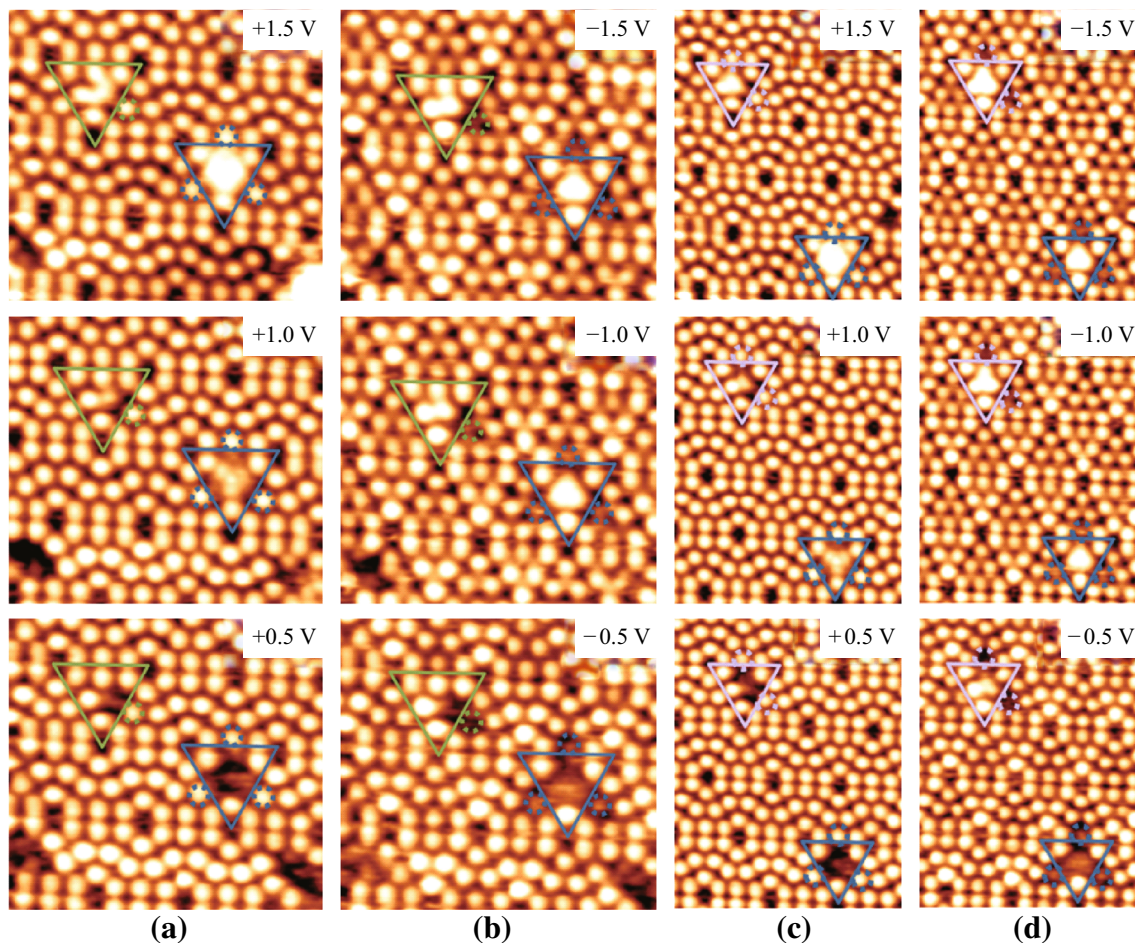
Fig. 2 Experimental empty (**a**, **c**) (9 nm × 9 nm) and filled (**b**, **d**) (9 nm × 11.5 nm) state STM images of three types of Zn-induced nanoclusters in the FHUCs recorded at bias voltages of +1.5, +1.0, +0.5, −0.5, −1.0, and −1.5 V, respectively. Three types of Zn-induced nanoclusters observed in Fig. 1b and c are denoted, respectively, by the *green*, *pink*, and *blue triangles*. The *closet* Si edge adatoms in neighboring UHUCs are denoted, respectively, by the *green*, *pink*, and *blue dotted circles*. (Color figure online)

unaltered Si edge adatom. The formation of type II nanocluster should be related to two Si edge adatoms and none of the other intact Si edge adatom in the FHUC. Different from the isosceles triangle pattern, the cluster exhibits an equilateral triangle pattern at the bias voltages of −1.5 and −1.0 V. As the voltage further reduces to −0.5 V, the cluster also transforms to the pattern with one bright dot and two almost absent Si edge adatoms. Three closet Si edge adatoms in the neighboring UHUCs show also almost unaltered images in the empty-state STM images as compared with the clean Si(111)-(7×7) surface. Only two of the three closet Si edge adatoms tune to be the dark pattern at a negative voltage of −0.5 V, and their positions are also just opposite of the dispersed Si edge adatoms in the FHUC. Therefore, similar to type I and III nanoclusters, the formation of type II nanocluster is obviously related to two displaced Si edge adatoms in the FHUC and the other one Si edge adatom is almost kept unaltered. Two base angles of the isosceles triangle at the bias voltage of +1.5 V, as

shown in Fig. 2c, could be deduced to be the two displaced Si edge adatoms. Similarly, the structural configuration of type II nanocluster is also not clear due to the uncertainty of the number and the position of adsorbed Zn atoms. But the above systematical structural analysis provides us the useful information for constructing preferable models for type I and II nanoclusters.

According to above structural information, type I nanocluster is related to one displaced Si edge adatom in the FHUC. Taking into account the bonding symmetry, two most possible cluster models of Zn_1Si_1 and Zn_3Si_1 (as shown in Fig. 3b) are constructed to be considered as type I nanocluster in the FHUC. In order to compare the stability of the proposed cluster structures, the adsorption energy $E_a(n)$ of the cluster is written as

$$E_a(n) = [E_{slab}(n) - E_{clean}]/n - E_{atom},$$

where $E_{slab}(n)$, E_{clean}, and E_{atom} are the total energies of the n adsorbates of the adsorbed surface, the clean surface, and
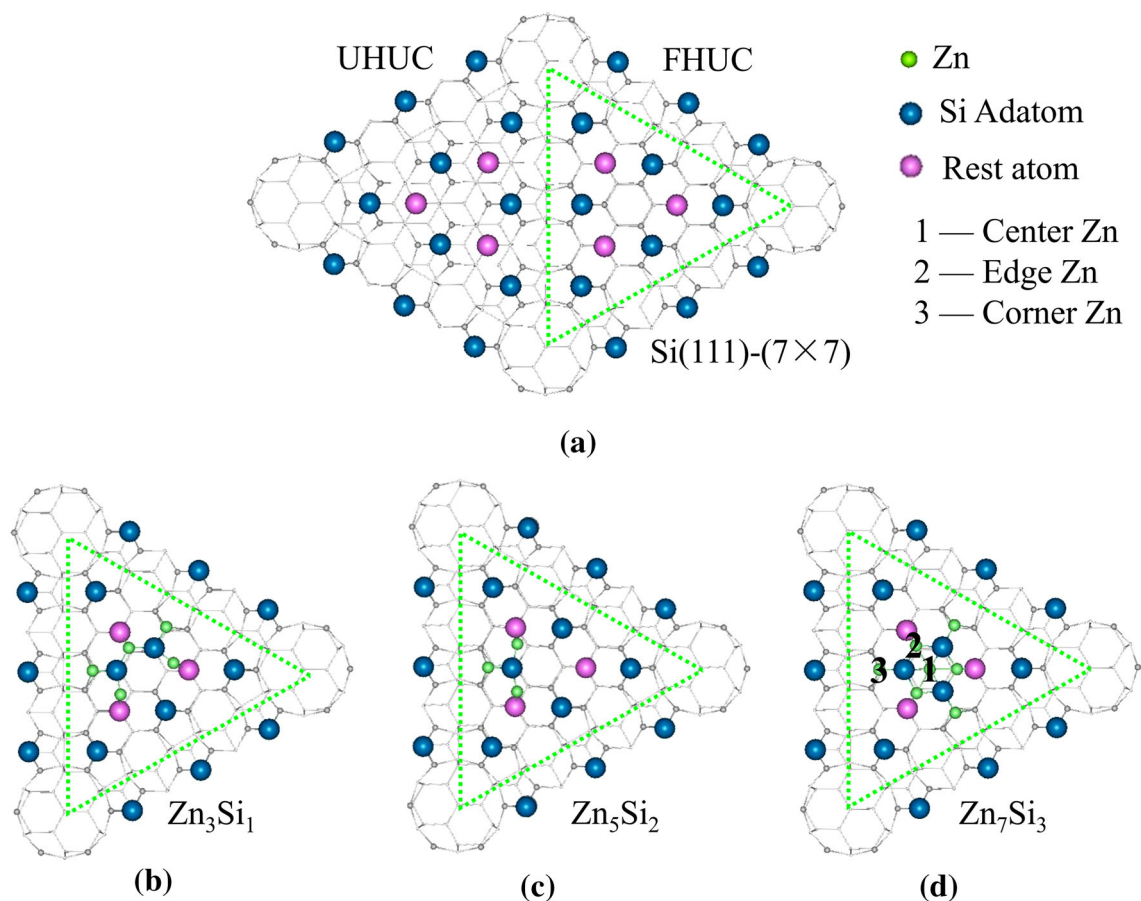
Fig. 3 **a** *Top view* of the DAS model of the Si(111)-(7×7) surface. **b**, **c**, and **d** are, respectively, the *top view* of the proposed Zn_3Si_1, Zn_5Si_2, and Zn_7Si_3 models in this work. The *green balls* are Zn atoms. The *blue* and *pink balls* are Si adatoms and rest atoms, respectively. The center, edge, and corner Zn atoms are marked as 1, 2, and 3, respectively. (Color figure online)

the isolated adsorbate atom, respectively [34]. Figure 4 aligns the calculated adsorption energies of the proposed Zn-induced nanoclusters. The calculated adsorption energy $E_a(n = 3)$ of Zn_3Si_1 structure is −1.416 eV/adatom, while that of Zn_1Si_1 $E_a(n = 1)$ is −0.124 eV/adatom. Therefore, the Zn_3Si_1 nanocluster is much more stable than Zn_1Si_1.
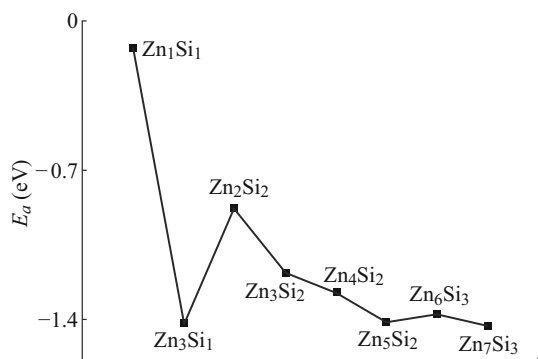
Fig. 4 The adsorption energies E_a of the proposed Zn-induced nanoclusters with the increasing of the Zn atoms

From the perspective of Zn–Si bonding, the atomic structure of Zn_3Si_1 cluster exhibits a characteristic of the valence. It is well known that the tetravalent Si adatoms and the rest atoms are partially filled, resulting in the dangling bonds on the Si(111)-(7×7) surface. As a transition group element, Zn likely has a variable valence state when reacting with nonmetallic atoms. Hence, in Zn_3Si_1 structure, one displaced Si edge adatom tends to bond with three Zn atoms and one Si atom below it. Consequently, the Zn_3Si_1 structure is relatively the stable configuration of Zn-induced nanoclusters on Si(111)-(7×7) surface with one displaced Si edge adatom in the FHUC.

Accordingly, type II nanocluster is related to two displaced Si edge adatoms in the FHUC. Therefore, four possible cluster structures of Zn_2Si_2, Zn_3Si_2, Zn_4Si_2, and Zn_5Si_2 (as shown in Fig. 3c) are constructed to be considered as this type of nanocluster in the FHUC. Zn_5Si_2 nanocluster has the lowest adsorption energy $E_a(n = 5)$ of −1.412 eV/adatom among the four possible clusters, as shown in Fig. 4. The lowest adsorption energy indicates that the Zn_5Si_2 nanocluster is the most stable atomic

structure among the three proposed configurations. Therefore, Zn_5Si_2 structure is relatively the stable configuration of Zn-induced nanoclusters on Si(111)-(7×7) surface with two displaced Si edge adatoms in the FHUC. In addition, the adsorption energy of Zn_5Si_2 is a little larger than that of Zn_3Si_1 structure. From the point of saturating the surface dangling bonds of Si edge adatoms, there are three Zn atoms bonding to one displaced Si edge adatom in a Zn_3Si_1 cluster. In a Zn_5Si_2 cluster, while there also are three Zn atoms binding to one displaced Si edge adatom, one of the five Zn atoms bind simultaneously to two displaced Si edge adatoms. Thus, with respect to the Zn_3Si_1 cluster, the five Zn atoms in Zn_5Si_2 cluster are insufficient for saturating two displaced Si edge adatoms, resulting in a little higher adsorption energy.

Based on above theoretical results, Zn_3Si_1 cluster is the most stable structure in the case of one displaced Si edge adatom, while Zn_5Si_2 cluster is the most stable structure in the case of two displaced Si edge adatoms. Furthermore, the adsorption energies of Zn_6Si_3 and Zn_7Si_3 clusters with three displaced Si edge adatoms are, respectively, calculated to be −1.372 and −1.430 eV/adatom, as shown in Fig. 4. Among the four cluster models just mentioned above, the adsorption energy of Zn_7Si_3 is the lowest, and therefore Zn_7Si_3 cluster is the most stable configuration adsorbed on Si(111)-(7×7) surface. Among the other three clusters, the adsorption energy of Zn_3Si_1 is 0.004 eV/adatom lower than that of Zn_5Si_2, while the adsorption energy of Zn_5Si_2 is curiously 0.04 eV/adatom lower than that of Zn_6Si_3. From the point of saturating the surface dangling bonds of Si edge adatoms, there are three Zn atoms bonding simultaneously to two displaced Si edge adatoms, therefore the highest adsorption energy of Zn_6Si_3 cluster can also be attributed to the insufficient saturation of the three displaced Si edge adatoms. As a result, Zn_3Si_1 and Zn_5Si_2 clusters are, respectively, the most stable structures in the case of one and two displaced Si edge adatoms, while Zn_7Si_3 cluster is the most stable structure in the case of three displaced Si edge adatoms. Moreover, the adsorption energy alignment in Fig. 4 shows that there are three minimal adsorption energies as the adsorbed Zn atoms increasing from one to seven. Thus, from the view point of the preferred energy, the most stable Zn_7Si_3 nanoclusters should grow up on the base of Zn_3Si_1 and Zn_5Si_2 clusters as the increasing of the adsorbed Zn atoms in the triangular half 7×7 unit cell. Furthermore, we compare the experimental distributions of these three kinds of Zn-induced nanoclusters at different coverage of Zn atoms. It is found that all the Zn_3Si_1, Zn_5Si_2, and Zn_7Si_3 clusters could be observed with the tiny number of Zn atoms adsorbed, and the Zn_3Si_1 and Zn_5Si_2 clusters gradually disappear when increasing the Zn deposition. As the content of Zn atoms further increases to 0.03 mL, almost no Zn_3Si_1 and

Zn_5Si_2 clusters are observed, while the surface is dominated by Zn_7Si_3 clusters, as shown in our previous work [14]. Therefore, we could deduce that, as the increasing of Zn deposition, the additional Zn atoms could gradually merge into the initially formed Zn_3Si_1 clusters, leading to the formation of Zn_5Si_2 and finally the Zn_7Si_3 clusters. In other words, the most stable Zn_7Si_3 nanocluster adsorbed on the Si(111)-(7×7) surface should be evolved continuously from Zn_3Si_1 and Zn_5Si_2 clusters.

It is known that STM actually probes the charge distribution near the Fermi level within an energy range determined by the sample bias. Therefore, Tersoff and Hamann [35] proposed that the STM images taken at different bias voltages could be simulated by integrating the partial charge densities in the energy window from the Fermi level to the sample bias. Thus, to further identify the configurations of the proposed Zn-induced nanoclusters and understand the evolution process at the different bias voltages, the topographic empty- and filled-state STM images of the clean, Zn_3Si_1, Zn_5Si_2, and Zn_7Si_3 nanoclusters-adsorbed Si(111)-(7×7) unit cells were further simulated, as shown in Fig. 5. For Zn_7Si_3 nanocluster-adsorbed Si surface, the filled-state images at the bias voltages of −1.5 and −1.0 V, only three displaced edge Si adatoms are visible, thus, the cluster appears as a big bright triangle. And at the bias voltages of ±0.5 V, all the Zn and Si atoms in the cluster are invisible. As the voltage increases to +1.0 V, the calculated empty-state images show typical tripod shape consisting of the center Zn atom and the three edge Zn atoms. Furthermore, in the neighboring uncovered UHUCs, the closest Si edge adatoms are almost darkened for all the filled-state STM images, comparing with the simulated STM image of clean Si(111)-(7×7). All above observed patterns based on the Zn_7Si_3 model are of remarkable quality, in agreement with the experimental images as shown in Fig. 2.

For the Zn_3Si_1 nanocluster, the empty-state image at the bias voltage of +1.5 V shows that the displaced Si adatom and two edge Zn atoms are visible, whereas the corner Zn atom is invisible, combined with two unaltered Si edge adatoms. The cluster appears as a "U" shape pattern in the center of FHUC. At the bias voltage of +1.0 V, only the displaced Si edge adatom is visible and the cluster changes to one dim dot. As the voltage further reduces to +0.5 V, all the Zn and displaced Si atoms made up of Zn_3Si_1 cluster are invisible. At the bias voltages of −1.5 and −1.0 V, only the displaced Si edge adatom is visible, combined with the other two unaltered Si edge adatoms, forming a "V" shape pattern in the center of FHUC. As the voltage further reduces to −0.5 V, the Zn_3Si_1 cluster is almost invisible, leaving two intact Si edge adatoms in the center of FHUC. Furthermore, the closet Si edge adatom in the neighboring UHUC, which just on the opposite of the
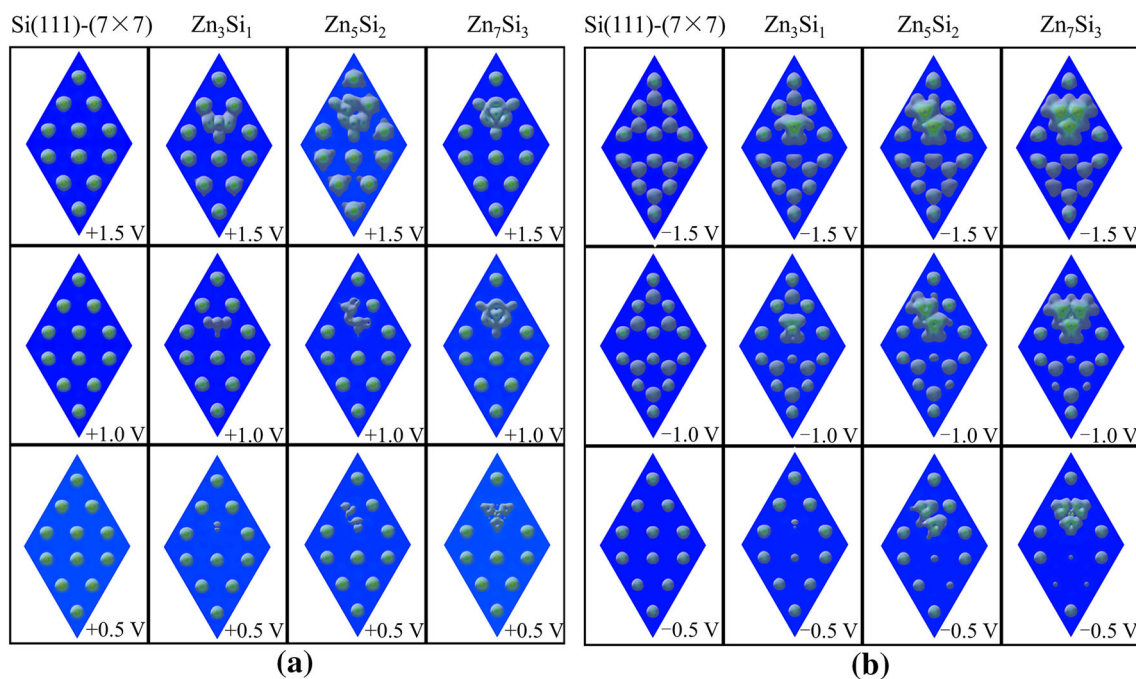
Fig. 5 The simulated empty (**a**) and filled-state (**b**) STM images of the clean, Zn_3Si_1, Zn_5Si_2, and Zn_7Si_3 nanoclusters-adsorbed Si(111)-(7×7) unit cells. The same bias voltages as in experiments (+1.5, +1.0, +0.5, −0.5, −1.0, and −1.5 V) are used in the calculations. The *colors* indicate the height of the images, *blue* being low and *yellow* being high. (Color figure online)

displaced Si edge adatom, exhibits dark images at the negative voltages. The suppression of the closest edge Si adatoms in the nearest neighboring uncovered UHUCs in filled-state STM images is mainly attributed to the displaced Si edge adatom, which is indicative of the charge transfer from the closest edge Si adatoms to the Zn nanocluster to further stabilize the cluster. Obviously, the simulated STM images of Zn_3Si_1 model in Fig. 5 are of remarkable quality, in agreement with the experimental results in Fig. 2a, which further demonstrates the rationality configuration for Zn_3Si_1 cluster.

For the Zn_5Si_2 nanocluster, the acquired STM image at the bias voltage of +1.5 V shows that two displaced Si edge adatoms are visible, combined with one unaltered Si edge adatom. The cluster displays as an isosceles triangular shape pattern forming in the center of FHUC. As the voltage reduces from +1.5 to +0.5 V, the size and brightness of the cluster decrease gradually and finally almost invisible, leaving one intact Si edge adatom in the center of FHUC. On the other hand, at the bias voltages of −1.5 and −1.0 V, only two displaced edge adatoms are acquired, combined with one other unaltered Si edge adatom, exhibiting as an equilateral triangle in the center of FHUC. As the voltage further reduces to −0.5 V, the cluster is almost invisible, leaving one intact Si edge adatom. Furthermore, at the negative voltages, two closet Si edge adatoms in the neighboring UHUC, which just on the opposite of the two displaced Si edge adatoms, exhibit two

dark dots with the comparison of clean Si(111)-(7×7) surface. The suppression of the closest edge Si adatoms in the nearest neighboring uncovered UHUCs in filled-state STM images is also related to the displaced Si edge adatoms. Thus, the simulated STM images of Zn_5Si_2 model in Fig. 5 are of remarkable quality, in agreement with the experimental results in Fig. 2b, which further demonstrates the rationality configuration for the Zn_5Si_2 cluster.

According to the above systematical analysis of the bias-dependent STM images, combined with the total energy calculation and accurate STM topographic simulation, the observed type I, II, and III nanoclusters, as denoted by the green, pink, and blue triangles in Fig. 1b and c, can reasonably be assigned as the Zn_3Si_1, Zn_5Si_2, and Zn_7Si_3 clusters, respectively. Moreover, from the view point of the preferred energy and the experimental distributions of these three Zn-induced nanocluster in different Zn coverage, we could deduce that the most stable Zn_7Si_3 nanocluster adsorbed on the Si(111)-(7×7) surface should be formed by the evolution of Zn_3Si_1 and Zn_5Si_2 clusters.

4 Conclusions

In summary, a tiny number of Zn atoms were deposited on Si(111)-(7×7) surface to study the evolution process of Zn-induced nanoclusters. The formation of type I, II, and III nanoclusters causes, respectively, one, two, and three

darkened closest Si edge adatoms in the neighboring UHUCs. The systematical bias-dependent structural analysis suggests that type III nanocluster is the Zn_7Si_3 cluster and the formation of type I and II nanoclusters is related to one and two displaced Si edge adatoms in the FHUC, respectively. First-principles adsorption energy calculations show that Zn_3Si_1 and Zn_5Si_2 clusters are, respectively, the most stable structures in the case of one and two displaced Si edge adatoms, while Zn_7Si_3 cluster is the most stable structure in the case of three displaced Si edge adatoms. Using the proposed structural models of Zn_3Si_1, Zn_5Si_2, and Zn_7Si_3, the simulated bias-dependent STM images are all well consistent with the experimental observations. Therefore, the observed type I, II, and III nanoclusters can reasonably be assigned as the Zn_3Si_1, Zn_5Si_2, and Zn_7Si_3 clusters, respectively. The most stable Zn_7Si_3 nanoclusters adsorbed on the Si(111)-(7×7) surface should grow up on the base of Zn_3Si_1 and Zn_5Si_2 clusters. A novel evolution process from Zn_3Si_1 to Zn_5Si_2, and finally to Zn_7Si_3 nanocluster is unveiled.

References

1. W.J. Cho, Y. Kim, J.K. Kim, Ultrahigh-density array of silver nanoclusters for SERS substrate with high sensitivity and excellent reproducibility. ACS Nano 6(1), 249–255 (2012). doi:10.1021/nn2035236

2. S.F. Li, X.J. Zhao, X.S. Xu, Y.F. Gao, Z.Y. Zhang, Stacking principle and magic sizes of transition metal nanoclusters based on generalized Wulff construction. Phys. Rev. Lett. 111(11), 115501 (2013). doi:10.1103/PhysRevLett.111.115501

3. M.C. Patterson, B.F. Habenicht, R.L. Kurtz, L. Liu, Y. Xu, P.T. Sprunger, Formation and stability of dense arrays of Au nanoclusters on hexagonal boron nitride/Rh(111). Phys. Rev. B 89(20), 205423 (2014). doi:10.1103/PhysRevB.89.205423

4. J. Pal, M. Smerieri, E. Celasco, L. Savio, L. Vattuone, M. Rocca, Morphology of monolayer MgO films on Ag(100): switching from corrugated islands to extended flat terraces. Phys. Rev. Lett. 112(12), 126102 (2014). doi:10.1103/PhysRevLett.112.126102

5. A.O. Orlov, I. Amlani, G.H. Bernstein, C.S. Lent, G.L. Snider, Realization of a functional cell for quantum-dot cellular automata. Science 277(5328), 928–930 (1997). doi:10.1126/science.277.5328.928

6. R.P. Andres, T. Bein, M. Dorogi, S. Feng, J.I. Henderson, C.P. Kubiak, W. Mahoney, R.G. Osifchin, R. Reifenberger, "Coulomb staircase" at room temperature in a self-assembled molecular nanostructure. Science 272(5266), 1323–1325 (1996). doi:10.1126/science.272.5266.1323

7. T.W. Kim, D.C. Choo, J.H. Shim, S.O. Kang, Single-electron transistors operating at room temperature, fabricated utilizing nanocrystals created by focused-ion beam. Appl. Phys. Lett. 80(12), 2168–2170 (2002). doi:10.1063/1.1458685

8. S.H. Sun, C.B. Murray, D. Weller, L. Folks, A. Moser, Monodisperse FePt nanoparticles and ferromagnetic FePt nanocrystal superlattices. Science 287(5460), 1989–1992 (2000). doi:10.1126/science.287.5460.1989

9. K. Koike, H. Matsuyama, Y. Hirayama, K. Tanahashi, T. Kanemura, O. Kitakami, Y. Shimada, Magnetic block array for patterned magnetic media. Appl. Phys. Lett. 78(6), 784–786 (2001). doi:10.1063/1.1345804

10. T. Koide, H. Miyauchi, J. Okamoto, T. Shidara, A. Fujimori, H. Fukutani, K. Amemiya, H. Rakeshita, S. Yuasa, T. Katayama, Y. Suzuki, Direct determination of interfacial magnetic moments with a magnetic phase transition in Co nanoclusters on Au(111). Phys. Rev. Lett. 87(25), 257201 (2001). doi:10.1103/PhysRevLett.87.257201

11. K.H. Wu, Y. Fujikawa, T. Nagao, Y. Hasegawa, K.S. Nakayama, Q.K. Xue, E.G. Wang, T. Briere, V. Kumar, Y. Kawazoe, S.B. Zhang, T. Sakurai, Na adsorption on the Si(111)-(7×7) surface: from two-dimensional gas to nanocluster array. Phys. Rev. Lett. 91(12), 126101 (2003). doi:10.1103/PhysRevLett.91.126101

12. J.R. Ahn, G.J. Yoo, J.T. Seo, J.H. Byun, H.W. Yeom, Electronic states of two-dimensional adatom gas and nanocluster array: Na on Si(111)7×7. Phys. Rev. B 72(11), 113309 (2005). doi:10.1103/PhysRevB.72.113309

13. Y.P. Wu, Y.H. Zhou, C.J. Zhou, H.H. Zhan, J.Y. Kang, Atomic structure and formation mechanism of identically sized Au clusters grown on Si(111)-7×7 surface. J. Chem. Phys. 133(12), 124706 (2010). doi:10.1063/1.3481483

14. C.J. Zhou, Q.K. Xue, J.F. Jia, H.H. Zhan, J.Y. Kang, Structural and electronic properties of identical-sized Zn nanoclusters grown on Si(111)-(7×7) surfaces. J. Chem. Phys. 130(2), 024701 (2009). doi:10.1063/1.3046682

15. J.F. Jia, J.Z. Wang, X. Liu, Q.K. Xue, Z.Q. Li, Y. Kawazoe, S.B. Zhang, Artificial nanocluster crystal: lattice of indentical Al clusters. Appl. Phys. Lett. 80(17), 3186–3188 (2002). doi:10.1063/1.1474620

16. R.W. Li, J.H.G. Owen, S. Kusano, K. Miki, Dynamic behavior and phase transition of magic Al clusters on Si(111)-7×7 surfaces. Appl. Phys. Lett. 89(7), 073116 (2006). doi:10.1063/1.2337522

17. V.G. Kotlyar, A.V. Zotov, A.A. Saranin, T.V. Kasyanova, M.A. Cherevik, I.V. Pisarenko, V.G. Lifshits, Formation of the ordered arrays of Al magic clusters on Si(111)7×7. Phys. Rev. B 66(16), 165401 (2002). doi:10.1103/PhysRevB.66.165401

18. M.Y. Lai, Y.L. Wang, Self-organized two-dimensional lattice of magic clusters. Phys. Rev. B 64(24), 241404 (2001). doi:10.1103/PhysRevB.64.241404

19. L. Vitali, M.G. Ramsey, F.P. Netzer, Nanodot formation on the Si(111)-(7×7) surface by adatom trapping. Phys. Rev. Lett. 83(2), 316–319 (1999). doi:10.1103/PhysRevLett.83.316

20. J.L. Li, J.F. Jia, X.J. Liang, X. Liu, J.Z. Wang, Q.K. Xue, Z.Q. Li, J.S. Tse, Z.Y. Zhang, S.B. Zhang, Spontaneous assembly of perfectly ordered identical-size nanocluster arrays. Phys. Rev. Lett. 88(6), 066101 (2002). doi:10.1103/PhysRevLett.88.066101

21. S.C. Li, J.F. Jia, R.F. Dou, Q.K. Xue, I.G. Batyrev, S.B. Zhang, Borderline magic clustering: the fabrication of tetravalent Pb

202

Nano-Micro Lett. (2015) 7(2):194–202

cluster arrays on Si(111)-(7×7) surfaces. Phys. Rev. Lett. **93**(11), 116103 (2004). doi:10.1103/PhysRevLett.93.116103

22. M.A.K. Zilani, H. Xu, T. Liu, Y.Y. Sun, Y.P. Feng, X.S. Wang, A.T.S. Wee, Electronic structure of Co-induced magic clusters grown on Si(111)-(7×7): scanning tunneling microscopy and spectroscopy and real-space multiple-scattering calculations. Phys. Rev. B **73**(19), 195415 (2006). doi:10.1103/PhysRevB.73.195415

23. M.A.K. Zilani, Y.Y. Sun, H. Xu, L. Liu, Y.P. Feng, X.S. Wang, A.T.S. Wee, Reactive Co magic cluster formation on Si(111)-(7×7). Phys. Rev. B **72**(19), 193402 (2005). doi:10.1103/PhysRevB.72.193402

24. J. Alvarez, A.L.V. Deparga, J.J. Hinarejos, J. Delafiguera, E.G. Michel, C. Ocal, R. Miranda, Initial stages of the growth of Fe on Si(111)7×7. Phys. Rev. B **47**(23), 16048–16051 (1993). doi:10.1103/PhysRevB.47.16048

25. M.K.J. Johansson, S.M. Gray, L.S.O. Johansson, Studies of low coverage adsorption of Li on Si(001): observation of negative differential resistance and electron trapping. J. Vac. Sci. Technol., B **14**(2), 1015–1018 (1996). doi:10.1116/1.588445

26. N.P. Guisinger, M.E. Greene, R. Basu, A.S. Baluch, M.C. Hersam, Room temperature negative differential resistance through individual organic molecules on silicon surfaces. Nano Lett. **4**(1), 55–59 (2004). doi:10.1021/nl0348589

27. J.P. Perdew, J.A. Chevary, S.H. Vosko, K.A. Jackson, M.R. Pederson, D.J. Singh, C. Fiolhais, Atoms, molecules, solids, and surfaces: applications of the generalized gradient approximation for exchange and correlation. Phys. Rev. B **46**(11), 6671–6687 (1992). doi:10.1103/PhysRevB.46.6671

28. Y. Wang, J.P. Perdew, Correlation hole of the spin-polarized electron gas, with exact small-wave-vector and high-density scaling. Phys. Rev. B **44**(24), 13298–13307 (1991). doi:10.1103/PhysRevB.44.13298

29. G. Kresse, D. Joubert, From ultrasoft pseudopotentials to the projector augmented-wave method. Phys. Rev. B **59**(3), 1758–1775 (1999). doi:10.1103/PhysRevB.59.1758

30. G. Kresse, J. Furthmüller, Efficient iterative schemes for ab initio total-energy calculations using a plane-wave basis set. Phys. Rev. B **54**(16), 11169–11186 (1996). doi:10.1103/PhysRevB.54.11169

31. G. Kresse, J. Furthmüller, Efficiency of ab initio total energy calculations for metals and semiconductors using a plane-wave basis set. Comput. Mater. Sci. **6**(1), 15–50 (1996). doi:10.1016/0927-0256(96)00008-0

32. M.C. Payne, M.P. Teter, D.C. Allan, T.A. Arias, J.D. Joannopoulos, Iterative minimization techniques for ab initio total-energy calculations: molecular dynamics and conjugate gradients. Rev. Mod. Phys. **64**(4), 1045–1097 (1992). doi:10.1103/RevModPhys.64.1045

33. K. Takayanagi, Y. Tanishiro, M. Takahashi, S. Takahashi, Structural analysis of Si(111)-7×7 by UHV-transmission electron diffraction and microscopy. J. Vac. Sci. Technol., A **3**(3), 1502–1506 (1985). doi:10.1116/1.573160

34. G. Lee, C.G. Hwang, N.D. Kim, J. Chung, J.S. Kim, S. Lee, Ab initio study of thallium nanoclusters on Si(111)-7×7. Phys. Rev. B **76**(24), 245409 (2007). doi:10.1103/PhysRevB.76.245409

35. J. Tersoff, D.R. Hamann, Theory of the scanning tunneling microscope. Phys. Rev. B **31**(2), 805–813 (1985). doi:10.1103/PhysRevB.31.805